

Article

Electrochemical Promotion of CO₂ Hydrogenation Using Rh Catalysts Supported on O²⁻ Conducting Solid Electrolyte

Nikoleta Kokkinou, Fotios Xydas, Susanne Brosda, Georgios Kyriakou  and Alexandros Katsaounis * 

Department of Chemical Engineering, University of Patras, Caratheodory 1, 26504 Patras, Greece

* Correspondence: alex.katsaounis@chemeng.upatras.gr

Abstract: Electrochemical promotion was used to modify the activity and selectivity of a Rh catalyst electrode in the CO₂ hydrogenation reaction. The experiments were carried out in a temperature range of 350–430 °C at ambient pressure and at different CO₂ to H₂ gas feeding ratios (1:2 to 4:1). The only reaction products observed were CO and CH₄, both under open- and closed-circuit conditions. The CH₄ formation rate was found to increase with both positive and negative potential or current application. The CO formation rate followed the opposite trend. The selectivity to CH₄ increased under high values of hydrogen partial pressure and decreased at high pressures of CO₂. The results demonstrate how electrochemical promotion can be used to finely tune activity and selectivity for a reaction of high technical and environmental importance.

Keywords: electrochemical promotion of catalysis (EPOC); non-faradaic electrochemical modification of catalytic activity (NEMCA); CO₂ hydrogenation; rhodium (Rh); YSZ; XPS

1. Introduction



Citation: Kokkinou, N.; Xydas, F.; Brosda, S.; Kyriakou, G.; Katsaounis, A. Electrochemical Promotion of CO₂ Hydrogenation Using Rh Catalysts Supported on O²⁻ Conducting Solid Electrolyte. *Catalysts* **2023**, *13*, 1014. <https://doi.org/10.3390/catal13061014>

Academic Editor: Giuseppe Bonura

Received: 18 May 2023

Revised: 6 June 2023

Accepted: 13 June 2023

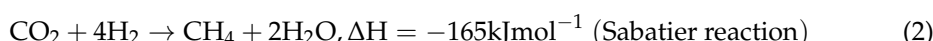
Published: 16 June 2023



Copyright: © 2023 by the authors. Licensee MDPI, Basel, Switzerland. This article is an open access article distributed under the terms and conditions of the Creative Commons Attribution (CC BY) license (<https://creativecommons.org/licenses/by/4.0/>).

Carbon dioxide (CO₂) is the most abundant greenhouse gas in our atmosphere with its concentration drastically increasing over time due to anthropogenic activities, most crucially the extensive use of fossil fuels for transport and power generation purposes. The ever-increasing CO₂ emissions in the atmosphere have gradually led to climate change, which is strongly associated with global warming, extreme weather conditions, and other major environmental threats [1–4]. In this regard, it is of foremost importance to globally minimize the use of fossil fuels, and accordingly, develop the necessary technologies for capturing and utilizing CO₂ to produce fuels, bulk chemicals, and value-added products. It is widely accepted that CO₂ hydrogenation may offer a relatively economic and effective way of controlling and making use of the CO₂ excess atmospheric levels [5–7].

Most studies of the catalytic hydrogenation of CO₂ have been performed in fixed-bed reactors using mainly metal catalysts (e.g., Rh, Pd, Ru, Cu, Fe, Co, Ni, Au, Ag) supported over a wide range of metal oxides (e.g., Nb₂O₅, ZrO₂, Al₂O₃, SiO₂) [8–37] and utilizing high pressures (5–70 atm) [12–15,17,24–28,30] which shift the thermodynamic equilibrium towards methanol and light hydrocarbon production. Under atmospheric pressure, CO₂ can be reduced by hydrogen to form methane (Sabatier reaction) and/or carbon monoxide (reverse water gas shift, RWGS, reaction) according to the following equations:



The RWGS reaction is endothermic and is thermodynamically favored at high operating temperatures. Contrary to this, the Sabatier reaction leads to the formation of methane, which is an exothermic reaction and is favored at low operation temperatures. However, the low operation temperatures limit the activity and the kinetics of the reactions as well.

Therefore, it is essential to develop active and selective low temperature catalytic processes, operating at high CO₂ to H₂ feed ratios and atmospheric pressure.

The electrochemical promotion of CO₂ hydrogenation has been studied in recent years over different catalytic films including noble and non-noble metals (Ru [7,38–43] and Rh [44,45], and Ni, Co, Fe [46,47], respectively) supported on a variety of solid electrolytes including yttria-stabilized-zirconia (YSZ, an O^{2−} conductor [7,38,44,45]), H⁺ conductors [40,43,46], and alkali ion conductors such as Na-β''-Al₂O₃ [40]. Under open circuit conditions, the non-promoted catalytic reaction takes place on the catalyst-working electrode. Application of a potential or current, between the catalyst film (working electrode) and a counter electrode, leads to changes of the conversion rate and product selectivity [7,38,48–56]. These non-Faradaic changes are evoked by the formation of an effective double layer due to the migration of promoting species (e.g., O^{2−} in the case of YSZ) migrating from the solid electrolyte to the metal–gas interface [7,38,49,57–59].

The CO₂ hydrogenation reaction on Rh catalyst-electrodes deposited on YSZ has been rarely investigated and mainly under conditions of excess of hydrogen (regarding Equation (1)) and cathodic polarizations. The study of the reaction in a single chamber reactor by Bebelis et al. [44] led to CO and CH₄ formation at temperatures of 346–477 °C. It was found that the rate of CH₄ formation is enhanced with positive potentials (electrophobic behavior) while the rate of CO formation is enhanced with negative potentials (electrophilic behavior). The maximum selectivity to CH₄ was up to 35%. Using a monolithic electro-promoted reactor (MEPR) [45], the reaction of CO₂ hydrogenation was studied on 22 thin Rh/YSZ/Pt plate cells at temperatures between 220 and 380 °C. The only products observed were, again, CO and CH₄. The rates of both reactions were significantly affected during polarization, while the selectivity to CH₄ remained always below 12%.

The pronounced catalytic activity of Rh-based catalysts, supported on O^{2−} conductors, under electro-promoted conditions have been associated in earlier studies with the decomposition of the rhodium oxide to metallic rhodium, which is more active especially under oxidation reaction conditions [57–59].

In the present study, the electrochemical promotion of CO₂ hydrogenation reaction was studied over a Rh catalyst-electrode deposited on an O^{2−} solid electrolyte conductor, YSZ, at atmospheric pressure, and for the first time, in a continuous single pellet flow reactor. The main scopes were in contrast to earlier studies: to perform CO₂ hydrogenation at a lower temperature range of 350–430 °C and at different CO₂ to H₂ cofeeding ratios.

2. Results and Discussion

2.1. Hydrogenation Activity Measurements

The steady-state-CO₂ conversion as a function of temperature for different CO₂ to H₂ ratios was first investigated. The results displayed in Figure 1 show that the conversion of CO₂ increases with increasing temperature reaching a maximum of 17.6% under reaction conditions of CO₂ to H₂ feeding ratio of 1:2. Under conditions of CO₂ to H₂ of 1:1 the conversion drops to 12% and is smallest with 6% and 2% at CO₂ to H₂ ratios of 2:1 and 4:1, respectively.

Figure 2 shows the CH₄ and CO production rates at steady state as a function of temperature. The rate of the methanation reaction was found to be highest for a gas feed ratio of CO₂ to H₂ of 1:2. With increasing CO₂ partial pressure in the reaction mixture, i.e., a CO₂ to H₂ ratio of 1:1, 2:1 and 4:1, the observed CH₄ formation rate is very low and almost independent of temperature. Figure 2b suggests that the RWGS reaction prevails over the Sabatier reaction. Moreover, as shown in Figure 3, CO appears to be the main product under all feeding CO₂ to H₂ ratios of this study and its selectivity is higher than 96%, while CH₄ selectivity is smaller than 4%. The reaction rate values of the RWGS reaction are more than one order of magnitude higher than those of the methanation one.

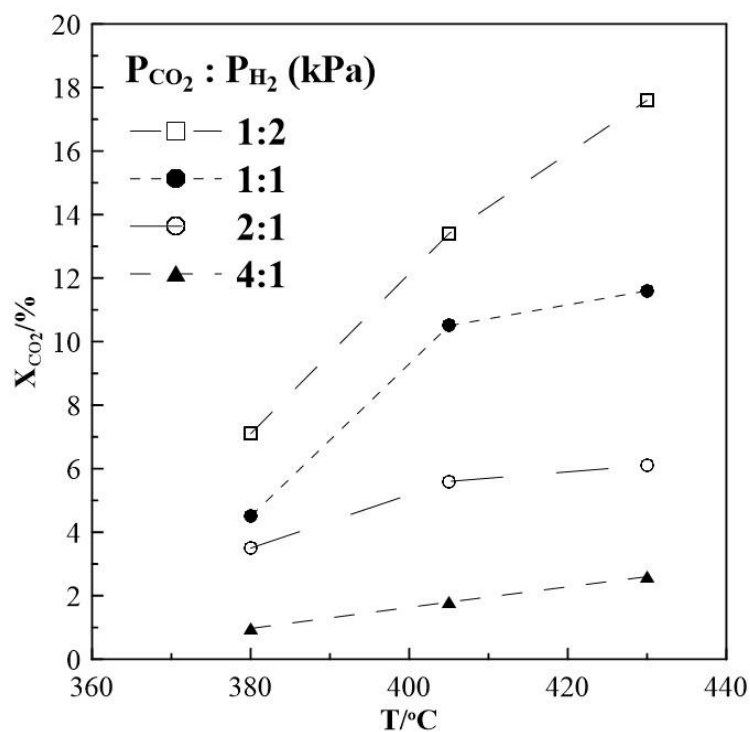


Figure 1. Steady-state effect of temperature on CO₂ conversion. Different gas feeding ratios of CO₂ to H₂. F_T = 50 cm³ min⁻¹.

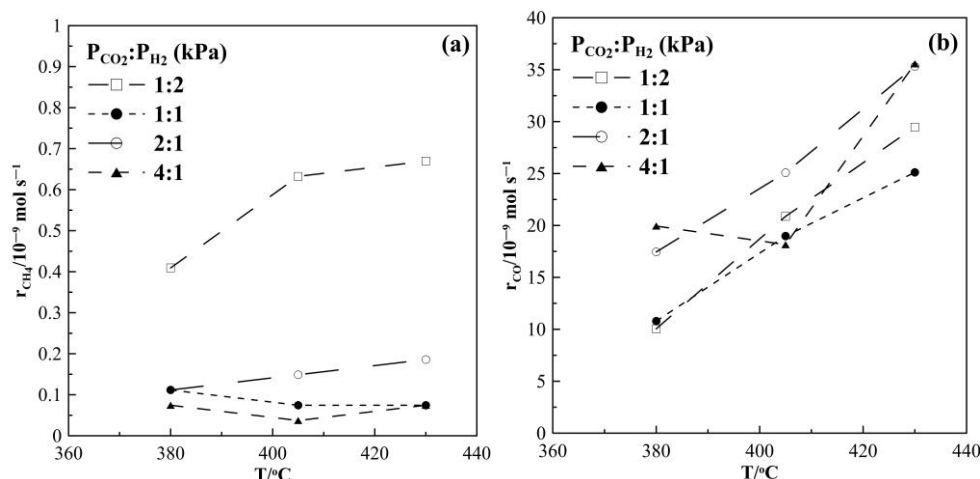


Figure 2. Steady-state effect of temperature on (a) CH₄ formation rate and (b) CO formation rate. Different gas feeding ratios of CO₂ to H₂. F_T = 50 cm³ min⁻¹.

Figures 4 and 5 depict the transient effect of constant applied positive (Figure 4) and negative (Figure 5) current on the catalytic rate and turnover frequency (TOF) for the formation of CH₄ and CO at a CO₂ to H₂ ratio of 1:2 at 380 °C. Initially, as presented in Figure 4, at t < 0, the circuit is open and the steady-state formation rates of CH₄ and of CO are equal to 0.38×10^{-9} mols⁻¹ and 9.2×10^{-9} mols⁻¹ respectively. At t = 0, a constant anodic current (I = +0.8 mA) is applied between the catalyst and counter electrode, which causes an applied potential of U_{WR} = +1.2 V. Oxygen ions, O²⁻, are transferred from the YSZ support to the Rh catalyst-electrode at a rate of I/2F equal to approximately 10^{-3} s⁻¹. The rate of CH₄ increases and approaches a new steady-state value ($r_{CH_4} = 0.62 \times 10^{-9}$ mols⁻¹). This increase of the CH₄ catalytic rate ($\Delta r = 0.24 \times 10^{-9}$ mols⁻¹) is 1.7 times greater than the initial rate achieved under open circuit conditions. The CO formation rate decreases under anodic current application to 8.0×10^{-9} mols⁻¹, resulting in a rate enhancement

value of $\rho = 0.84$. After current interruption, the CH_4 rate of formation returns to its initial open circuit value (reversible behavior), while the CO formation rate returns only to a value above the initial open circuit rate (non-reversible behavior). A very similar trend is observed under cathodic current application, as shown in Figure 5. The decrease in CO formation rate is less pronounced with a rate enhancement ratio, ρ , (see Equation (5) in Section 3.3) equal to 0.94. After current interruption, the rate does not return to its initial open circuit value. Under cathodic current application, CH_4 formation rate is increased and a rate enhancement ρ -value of 2.7 is estimated.

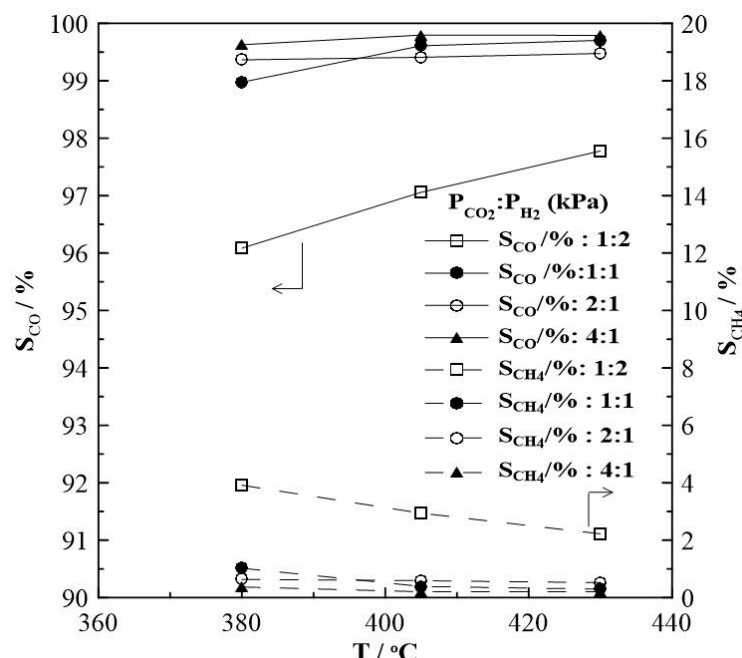


Figure 3. Steady-state effect of temperature on the selectivity to CO and CH_4 formation under open circuit conditions and at different gas feeding ratios of CO_2 to H_2 . $F_T = 50 \text{ cm}^3 \text{ min}^{-1}$.

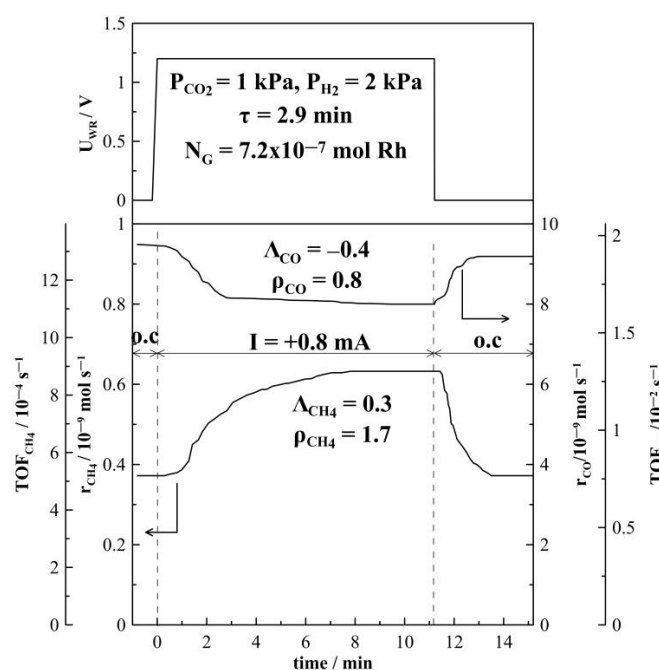


Figure 4. Transient effect of constant applied current ($I = +0.8 \text{ mA}$) on the formation rate of CH_4 and CO at $T = 380^\circ\text{C}$ and CO_2 to H_2 ratio of 1:2. $F_T = 50 \text{ cm}^3 \text{ min}^{-1}$.

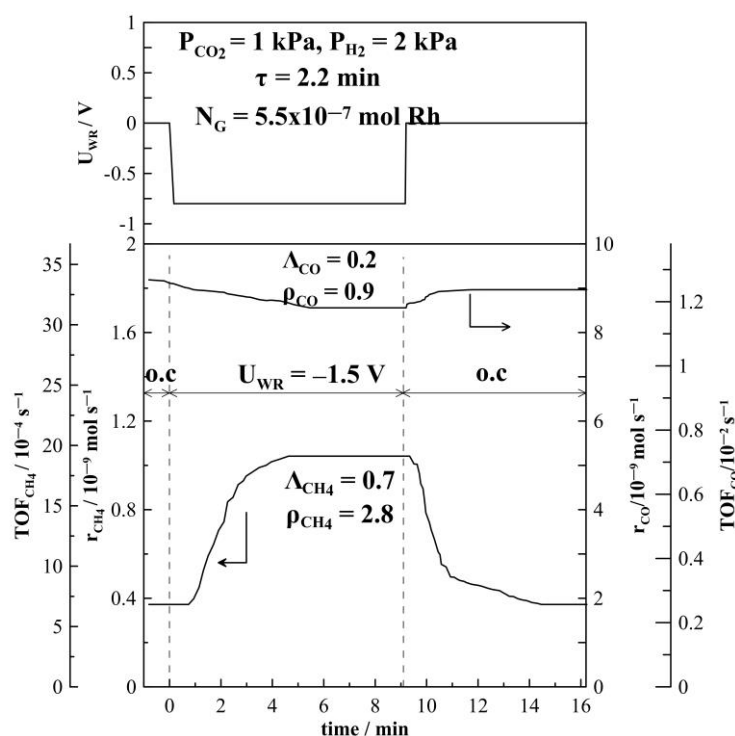


Figure 5. Transient effect of constant applied current ($I = -0.8$ mA) on the formation rate of CH_4 and CO at $T = 380$ $^{\circ}\text{C}$ and CO_2 to H_2 ratio of 1:2.

The time constant, τ , given in both Figures 4 and 5, is defined as the time required for the rate increase Δr to reach 63% of its new steady-state value during a galvanostatic transient [38,59]. When an O^{2-} ion conductor is used, the magnitude of τ can be generally predicted by

$$\tau \approx \frac{2FN_G}{I} \quad (3)$$

where N_G (mol) is the reactive oxygen uptake on the metal catalyst. The time constant τ expresses the time required to form a monolayer of $\text{O}^{\delta-}$ on the metal surface, while N_G expresses, approximately, the surface mols of metal—here, Rh. The average active catalyst surface area, N_G , which is equal to 7.62×10^{-7} mol Rh, has been calculated based on 6 galvanostatic transients. The estimated value of N_G agrees well with the values found in previous studies of Rh catalyst electrodes supported on YSZ [44,45,56,59]. The average N_G value obtained was used to calculate turnover frequencies (TOFs) for CH_4 and CO formation. TOFs for CH_4 formation are found to be small and in the order of 10^{-4} s^{-1} , which is in good agreement with the literature data [21].

The non-reversible behavior of CO formation has been further investigated by repeated current and/or potential application, which have generally shown that upon current and/or potential interruption the rate of CO formation does not return to its initial open circuit value. Figure 6 summarizes the results for potentiostatic transient operation at different CO_2 to H_2 feed ratios. The bottom part of the figure shows that the increase in CH_4 formation rate under anodic and cathodic polarization (+ and -1.5 V), which is more pronounced at high H_2 to CO_2 feeding ratios, is reversible. However, the CO formation rate, as shown in the top part of Figure 6, exhibits a “permanent”, non-reversible NEMCA behavior [60,61]. The guide (dotted) lines clearly show that this non-reversible effect of current and/or potential application is more pronounced at higher CO_2 to H_2 feed ratios.

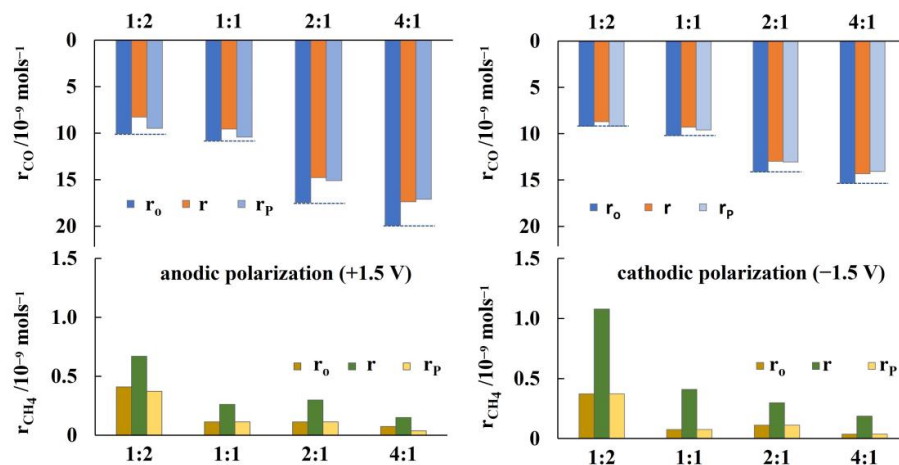


Figure 6. Transient effect of constant applied potential (left +1.5 V, right −1.5 V) on the formation rates of CH_4 and CO at $T = 380\text{ }^\circ\text{C}$ and at different ratios of CO_2 to H_2 . Dotted lines in the sketch for the CO formation rates point guidance for the non-reversible behavior of the open circuit rate after potential interruption, for details see text. $F_T = 50\text{ cm}^3\text{ min}^{-1}$. r_o is the formation rate under open circuit conditions, r is the formation rate under potentiostatic polarization, and r_p corresponds to the formation rate after potential interruption.

The “permanent” rate enhancement ratio γ , was defined for the first time by Comninellis et al. [61] as

$$\gamma = r_p / r_o \quad (4)$$

where r_p is the “permanent” promoted catalytic rate after current or potential interruption, and r_o is the unpromoted rate (i.e., the open-circuit catalytic rate). Figure 7 displays the non-reversibility magnitude of CO formation for different gas feed ratios. Under reaction conditions of a CO_2 to H_2 ratio of 1:2, the γ/ρ ratio is higher than 1, expressing, that the CO formation rate observed under potential application partially returns to its initial open circuit value. However, γ/ρ ratio equals to 1 for a reaction mixture with a CO_2 to H_2 ratio of 4:1 and a significant “permanent” NEMCA behavior is observed.

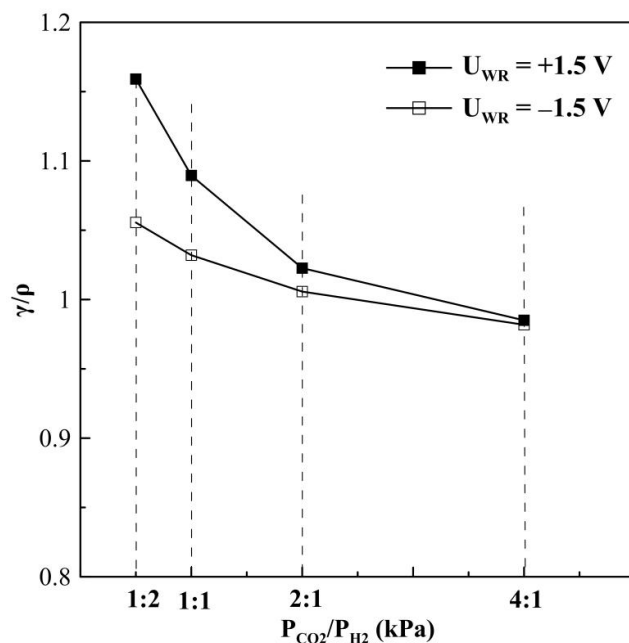


Figure 7. Ratio of “permanent” rate enhancement γ to rate enhancement ρ for CO formation at different gas feeding ratios, $T = 380\text{ }^\circ\text{C}$.

In the general case of an oxidation reaction on catalysts deposited on O²⁻ conductors, like YSZ, the ionic species migrating in the solid electrolyte is participating in the electrochemical reaction leading to distinct values of apparent Faradaic efficiency, $|\Lambda| > 1$ (see Equations (6)–(8), Section 3.3). In the present case, however, in which oxygen is not a reactant, any positive current or positive potential-induced catalytic rate change denotes electrochemical promotion, even when $|\Lambda| < 1$ [39].

Figure 8 summarizes the results of steady-state potential application on the rate of CH₄ formation at T = 430 °C, for which the highest rate enhancement ratio, ρ has been found. The observed currents do not depend on gas feed conditions, which means they are almost equal at a given potential and do not depend on the CO₂ to H₂ ratios. This observation is one of the very first hints that the overall oxidation state of the film remains relatively unchanged during the course of the reaction. The rate of CH₄ production displays an inverted volcano type behavior, i.e., it increases with increasing and decreasing catalyst potential as shown in Figure 8a. Maximum changes in the CH₄ rate are observed under reaction conditions of a CO₂ to H₂ ratio of 1:2, but the highest rate enhancement ratios are achieved at conditions of CO₂:H₂ = 1:1, with ρ reaching values of up to 11. If the partial pressure of CO₂ is further increased, i.e., CO₂ to H₂ ratios of 2:1 and 4:1, methane formation is found to be small with values below 0.6 × 10⁻⁹ mol s⁻¹. Despite this, however, methane formation can be electrochemically promoted with ρ -values of up to 5. Product selectivity towards CH₄ is electrochemically promoted under anodic and cathodic polarization; furthermore, it is highest under reaction conditions of a CO₂ to H₂ ratio of 1:2, but does not exceed 10%, as seen in Figure 9.

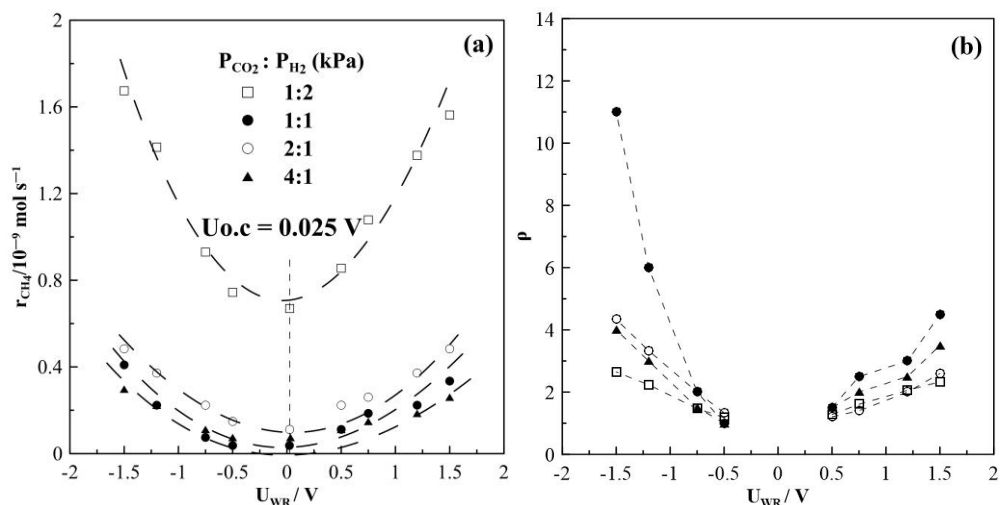


Figure 8. Steady-state effect of potential on (a) CH₄ formation rate and (b) the corresponding rate enhancement ratio, T = 430 °C, different gas feeding ratios, F_T = 50 cm³ min⁻¹.

2.2. Catalyst Characterization

The morphology and chemical state of the Rh/YSZ film was assessed with XRD (X-ray diffraction), SEM (scanning electron microscopy) and XPS (X-ray photoelectron spectroscopy). The characterization studies were carried out on 2 different samples, designated as fresh and used, which correspond to the freshly reduced (i.e., after treatment in 15% H₂ in He) and a post-experiment (i.e., after exposure to different CO₂: H₂ gas feed compositions) Rh/YSZ catalyst electrode, respectively.

The diffractograms displayed in Figure 10 show no major differences in the phase distribution of the fresh and used sample. More specifically both diffractograms show clear reflections at $2\theta = 30.3^\circ, 35.0^\circ, 50.4^\circ, 59.9^\circ, 62.9^\circ, 74.1^\circ$, and 81.9° , which correspond to the (111), (200), (220), (311), (222), (400), (331) planes of YSZ [62–67]. In addition, both diffractograms show clear reflections at $41.5^\circ, 48.4^\circ$, and 70.7° which correspond to the (111), (200), and (220) phases Rh particles in their metallic (Rh⁰) state [66]. No reflections

corresponding to RhO_2 or Rh_2O_3 were detected in the XRD measurements, suggesting that the chemical state of the Rh film is mostly metallic before and after use.

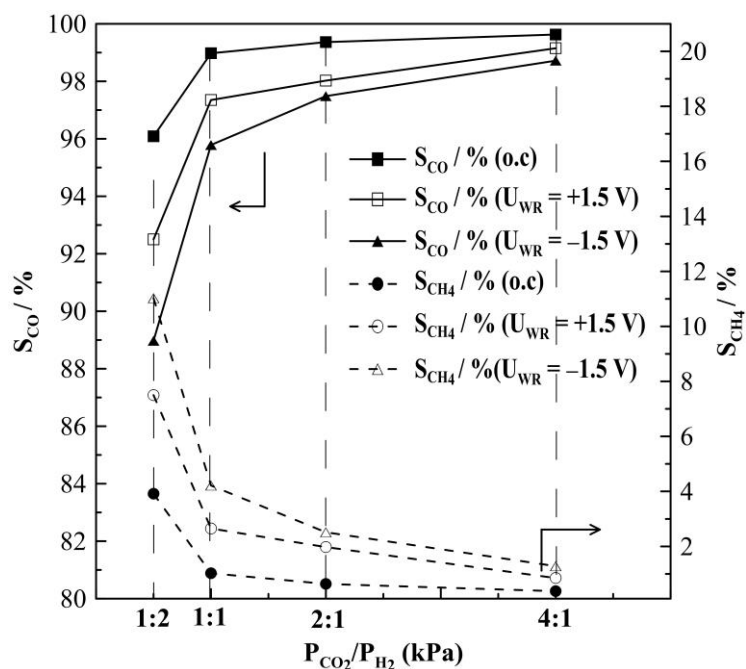


Figure 9. Steady-state effect of gas feeding ratios of CO_2 to H_2 on the selectivity to CO and CH_4 formation on Rh catalyst under open and closed-circuit conditions, $T = 380 \text{ }^\circ\text{C}$.

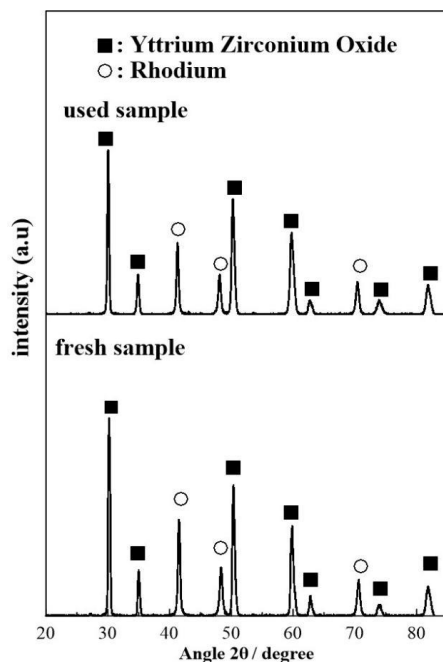


Figure 10. XRD patterns of the freshly reduced and used (after exposing to experimental operating conditions) sample.

The mean Rh crystallite size of the fresh and used samples were calculated by means of the Scherrer equation [65] by assuming a spherical crystallite shape and averaging the crystalline domain diameter obtained for the (111), (200), and (220) reflections. The size of the Rh crystallites in the fresh sample ($19.9 \pm 0.8 \text{ nm}$) was found to be slightly smaller as compared to the used sample ($24 \pm 1 \text{ nm}$), which suggests that some degree of crystallite size increase during the course of the electrocatalytic reaction due to agglomeration.

Previous XRD studies on Rh/YSZ systems have shown that after reduction and prior to experimental measurements the metallic phase of Rh is mainly present in the sample with only tracers of metal oxides being detectable [66]. Using metalorganic paste (Engelhard 8826) as a precursor, Jimenez et al. reported rhodium crystallite sizes equal to 58.5 ± 0.3 nm, calculated by the XRD patterns of the reduced sample [66]. The observed size variation and the Rh⁰: Rh oxide ratio were attributed to the different conditions of calcination and reduction conditions of the working Rh-catalyst electrode.

Top view and cross section SEM images of the fresh and used catalyst film are shown in Figures 11 and 12, respectively. Overall, the sample preparation method followed in this work has led to a continuous rhodium film, sufficiently porous which facilitates the efficient access of both reactants and products on the Rh active sites, and well attached to the YSZ support to ensure an electrochemically active interface. The apparent average particle size is estimated to be 40 nm, which is roughly twice the crystallite size calculated from the XRD spectra. It is worth mentioning here that particle size estimation from the SEM images is limited by the resolution of the instrument. Both the morphology and structure of the Rh film appears to be unchanged comparing the images from the sample prior experiment and after exposing it to reaction conditions. The thickness of the catalyst film was estimated from the cross-section micrograph and was found to be in the range of 6.5–10 μ m, which is a common thickness for films prepared by applying metalorganic pastes [38].

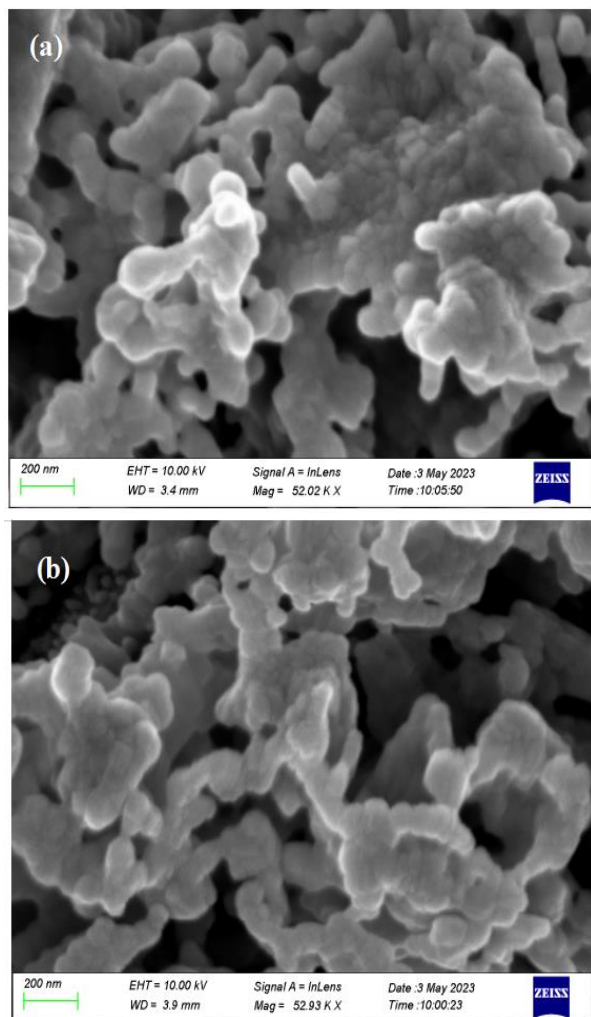


Figure 11. SEM micrographs of Rh/YSZ from top view (a) fresh sample and (b) used sample.

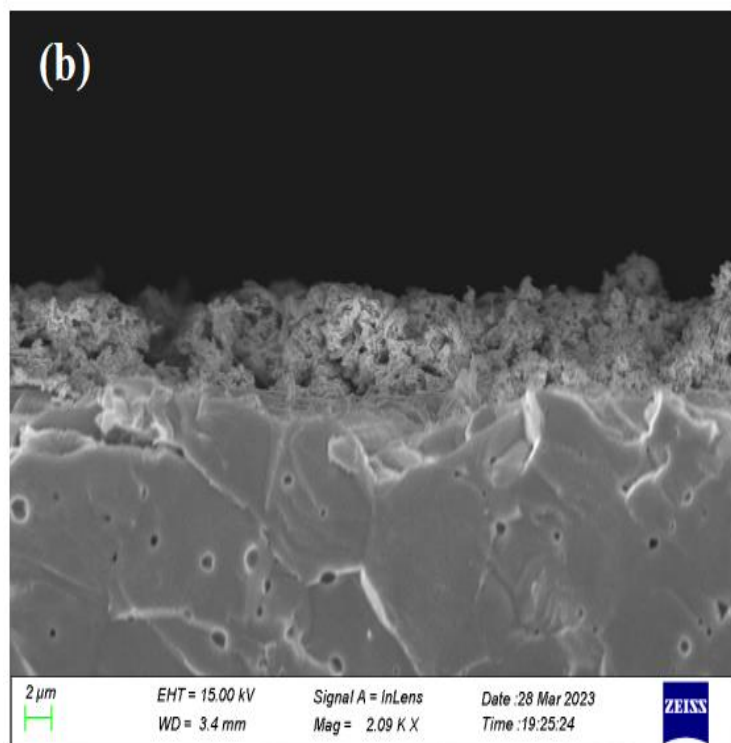
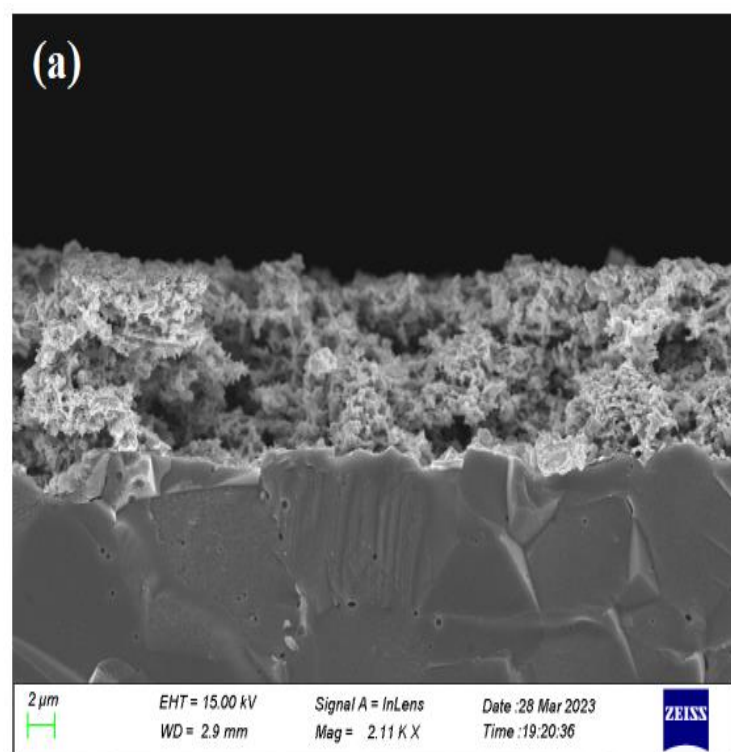


Figure 12. SEM micrographs of Rh/YSZ from cross section (a) fresh sample and (b) used sample.

Figure 13a shows the Rh 3d spectra of the freshly reduced and post-reaction (used) sample. The Rh 3d_{5/2} peak of the fresh sample is centred at approximately 307.2 eV, which indicates that the Rh catalyst film is mostly in the metallic state, without excluding the possibility of some minor Rh oxide quantities being also present [66]. The post-reaction data suggest that the surface chemical state of the Rh electrocatalyst film has not changed significantly. A rather small shift of ~0.2 eV towards lower binding energy is observed

suggesting that a minor oxide component may be present in the fresh sample which has been reduced after reaction leading to the apparent shift. To clarify this point, the raw Rh3d spectra were deconvoluted using an asymmetric peak shape for the metallic state and Gaussian–Lorentzian peak shape for the oxidized state. Figure 13a shows that the metallic Rh3d_{5/2} component (solid line) is centred at ~307 eV while the oxidized Rh3d_{5/2} component (dashed line) is centred at ~308 eV. The ratio of metallic Rh to oxidized Rh is 1:9, confirming that Rh film is nearly metallic both before and after reaction. It is worth noting here that the post-reaction spectra have been acquired after testing the catalyst under reaction conditions of CO₂ to H₂ of 1:4. The XPS results are in close agreement with the XRD data presented above (Figure 10), with the two techniques suggesting the absence of any substantial quantity of Rh oxide on the surface or bulk of the Rh film. Minor quantities of carbon were present on both the fresh and used samples (Figure 13b). More crucially, the amount of carbon was not found to increase in the post-reaction sample, which indicates that there is no carbon deposition on the catalyst surface during the reaction, especially under feed conditions of P_{CO₂}:P_{H₂} ratios of 4:1.

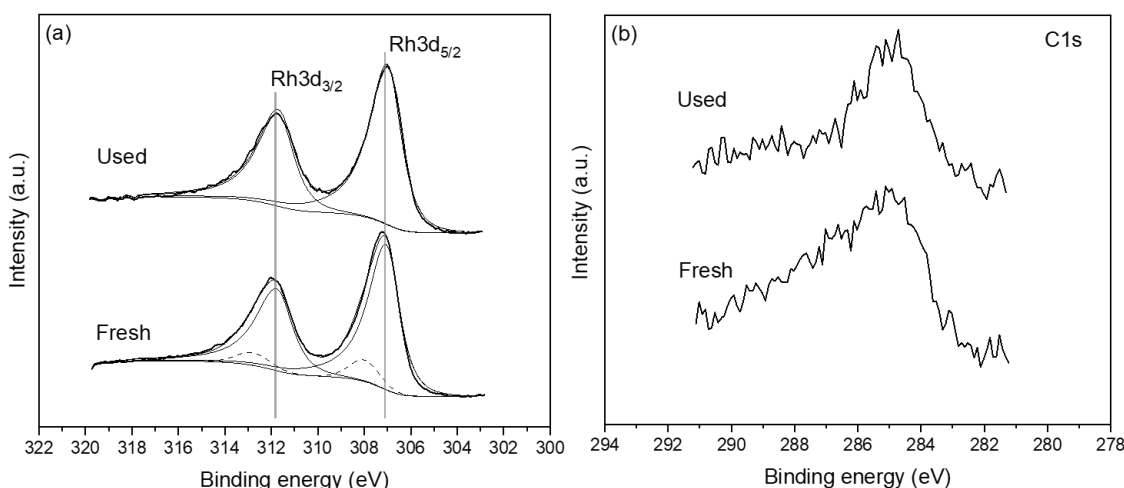


Figure 13. XPS measurements of the freshly reduced and post-reaction used catalyst sample. (a) Rh 3d and (b) C 1s regions.

3. Experimental

3.1. Catalyst Preparation

A disc of 8% mol Y₂O₃-stabilized ZrO₂ (YSZ), with 17 mm diameter and 1.5 mm thickness, respectively, was utilized as solid electrolyte. Gold (Au) reference and counter electrodes were deposited on one side of the electrolyte, using Au paste (Metalor, AU 201 Gold Resinate, Birmingham, UK) and calcination at 450 °C for 30 min following a sintering at 700 °C for 1 h, with a heating rate of 10 °C min^{−1}.

The working electrode (Rh catalyst electrode) was deposited on the opposite side of the YSZ solid electrolyte by application of thin coatings of Rh paste (Engelhard Rhodium Resinate 8826, Cinderford, UK). Calcination was carried out in air at 550 °C for 3 h with a heating rate of 10 °C min^{−1}. Prior electrochemical experiments, the Rh catalyst electrode was reduced at 440 °C for 2 h under a flow of 15% H₂ in He. The total mass of the Rh catalyst electrode was 1.8 mg.

3.2. Reactor Operation

The electrocatalytic experiments were carried out in a continuous single pellet flow reactor, which has been discussed previously [38–40]. The feed gas composition and total flow rates were controlled by a set of electronic flow meters (Brooks Instrument, Hatfield, PA, USA). Reactants were certified standards of 5% CO₂ in He and 15% H₂ in He. Pure He (99.999%) was fed to further adjust the total flow rate and the inlet gas composition at the

desired values. Electrochemical experiments were performed at ambient pressure. Feed reactant partial pressure was varied between 1 to 4 kPa CO₂ and 1 to 7 kPa H₂.

The concentrations of reactants and products were analyzed with an IR CO₂-CO-CH₄ gas analyzer (Futzi Electric ZRE, Shinagawa City, Tokyo, Japan). Constant currents and potentials were applied using an AMEL 2053 galvanostat-potentiostat. CO₂, CO, and CH₄ were further analyzed by gas chromatography (Gas Chromatographer, Shimadzu 2014, Kyoto, Japan) with TCD and FID detectors, using a Porapak QS packed column.

Blank experiments have been carried out to confirm the non-catalytic behavior of the Au counter and reference electrodes under open- and closed-circuit conditions. For this purpose, an electrochemical cell of the type Au/YSZ/Au (replacing the Rh working electrode with Au) was investigated under reaction conditions of this study (T = 400 °C, F_T = 100 cm³ min⁻¹ and different H₂ to CO₂ gas feeding ratios). The obtained CO formation rate on Au was small with values of $r_{CO} < 10^{-9}$ mols⁻¹ and it was not affected by potential application. CH₄ formation on Au was not observed.

3.3. Electrochemical Promotion Parameters Computation

Figure 14 shows a schematic representation of the (Rh | YSZ | Au) electrochemical cell under (a) open circuit and (b) closed circuit conditions. WE correspond to the working electrode (Rh deposited catalytic active film), CE to the counter, and RE to the reference electrodes both made out of Au in order to be catalytically inactive. All 3 electrodes are deposited on yttria-stabilized zirconia (YSZ) which serves as a solid O²⁻ ion conductor at operating temperatures of 380 to 430 °C. Under open circuit conditions (i.e., no current passing through the cell), H₂ and CO₂ are co-fed over the conductive catalyst film leading to the formation of CO and CH₄, expressed by the unpromoted catalytic rate, r_0 . Under, for example, anodic polarization, the application of a positive potential between the counter and working electrode, O²⁻ ions from the solid electrolyte are migrating to the catalyst-film forming at the metal gas interface an effective double layer, that alters the catalytic activity, and leading to the electropromoted rate, r .

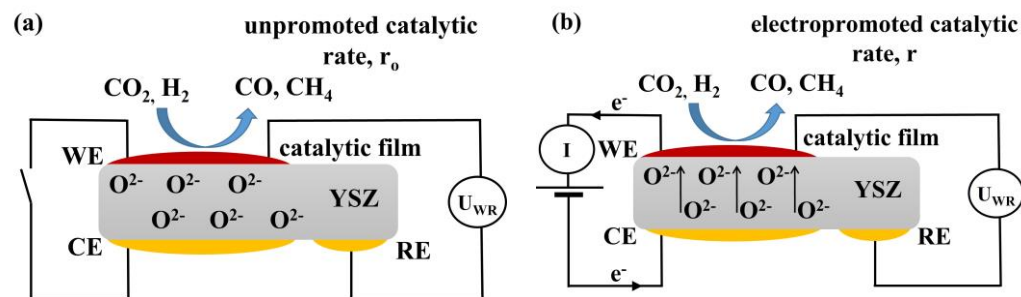


Figure 14. Schematic presentation of the electrochemical cell under (a) open and (b) closed circuit conditions, WE corresponds to the working electrode, CE to counter, and RE to reference electrode.

The non-Faradaic behavior is defined by two basic parameters, the rate enhancement ratio, ρ ,

$$\rho = \frac{r}{r_0} \quad (5)$$

where r is the electropromoted catalytic rate under polarization and r_0 is the unpromoted rate (i.e., the open-circuit catalytic rate). The apparent Faradaic efficiency, Λ , defined from:

$$\Lambda = \frac{\Delta r}{I/nF} \quad (6)$$

where Δr is the current- or potential-induced observed change in catalytic rate ($\Delta r = r - r_0$), I is the applied current, n is the number of exchanged electrons, and F is Faraday's constant.

In this study, where CH_4 and CO were the only products of the CO_2 hydrogenation reaction, the Faradaic efficiency for each formation reaction can be defined from the follow equations:

$$\Lambda_{\text{CO}} = \frac{2\Delta r_{\text{CO}} \left(\text{in} \frac{\text{mol}}{\text{s}} \right)}{I/F} \quad (7)$$

$$\Lambda_{\text{CH}_4} = \frac{8\Delta r_{\text{CH}_4} \left(\text{in} \frac{\text{mol}}{\text{s}} \right)}{I/F} \quad (8)$$

3.4. Catalyst Characterization

Wide-angle X-ray diffraction (XRD) patterns were recorded using a Bruker D8 Advance system equipped with Cu-K α radiation ($\lambda = 1.5418 \text{ \AA}$). The voltage and lamp current were adjusted to 40 kV and 40 mA, respectively. The angle range 2θ was 20–90° and scan speed was 0.3 s/step (Siemens D-500, Frankfurt, Germany).

High resolution field-emission scanning electron microscopy (FE-SEM) was employed using a Zeiss SUPRA 35VP system operating at 10–15 kV voltage range (Carl Zeiss AG, Jena, Germany).

Ex situ X-ray photoelectron spectroscopy (XPS) measurements of the fresh Rh catalyst sample (after H_2 reduction) and post-experiment sample were carried out in an ultrahigh-vacuum (UHV) system described in detail elsewhere [68]. Measurements were carried out using non-monochromatic AlK α radiation (1486.6 eV) and a Leybold LH EA11 energy analyzer (Leybold, Germany), which was operated at a constant pass energy (100 eV). The analyzed sample area was a $2 \times 5 \text{ mm}^2$ rectangle. All spectra were corrected for charge transfer using the C1s peak at 284.8 eV for adventitious carbon

4. Conclusions

In this work, the electrochemical promotion of CO_2 hydrogenation was studied over a Rh/YSZ electrode in a continuous single pellet flow reactor for $P_{\text{CO}_2}/P_{\text{H}_2}$ gas feed mixtures ranging from 1:2 to 4:1. Despite the large body of literature on the use of Rh/YSZ electrodes for other reactions such as NO reduction and ethylene oxidation under various experimental set-ups, CO_2 hydrogenation has been rarely investigated on Rh/YSZ using laboratory reactors. There are only a couple of references discussing data under reaction conditions of a narrow CO_2 to H_2 ratio of 1–1.5 or 1:1.8 and cathodic polarizations. The results of the present study show that potential or current application can strongly affect the CO_2 hydrogenation reaction, both in regard to the catalytic rates obtained but also selectivity to reactions products. In the temperature range of 350 to 430 °C, under atmospheric total pressure and with a total flowrate of $F_T = 50 \text{ cm}^3 \text{ min}^{-1}$, the only products found were CH_4 and CO. Increasing or decreasing the catalyst potential by up to 1.5 V leads to an inverted volcano type behavior of the methanation rate (the formation rate increases with anodic and cathodic polarization), while the rate of CO production follows a volcano type behavior (the formation rate decreases with anodic and cathodic polarization). The observed trends are confirmed by kinetic measurements and agree with the rules governing the EPOC phenomenon as described in bibliography.

The observed rate changes were non-faradaic and after current interruption, the catalytic rate of CH_4 formation returned to its initial open circuit value, demonstrating the reversibility of the phenomenon. However, the CO formation rate, exhibited a partial non-reversible behavior, which is more pronounced under a gas feed composition of CO_2 to H_2 ratio of 4:1., i.e., in excess of CO_2 . Permanent EPOC behavior was discussed in view of the stabilization of the Rh metallic phase under anodic polarization. Our preliminary XPS studies show that for pre- and post-reaction samples the Rh metal phase is mainly present, even after exposing the Rh film to higher CO_2 to H_2 ratios. This confirms that, at first glance, the partially permanent EPOC behavior in our case is due to the electrochemically induced stabilization of the Rh metallic phase.

Author Contributions: Conceptualization, A.K. and S.B.; methodology, S.B., G.K. and A.K.; investigation, N.K. and F.X.; resources, N.K., F.X. and S.B.; data curation, N.K. and F.X.; writing—original draft preparation, N.K. and S.B.; writing—review and editing, S.B., G.K. and A.K.; supervision, S.B., G.K. and A.K.; funding acquisition, G.K. and A.K. All authors have read and agreed to the published version of the manuscript.

Funding: NK thanks the National Scholarship Foundation (IKY) for financial support through the Program code: 5113934.

Data Availability Statement: All the experimental data presented in the current manuscript.

Acknowledgments: Authors are thankful to Panagiota Natsi for XRD patterns, and FORTH ICE-HT for SEM images.

Conflicts of Interest: The authors declare no conflict of interest.

References

1. Kinney, P.L. Interactions of Climate Change, Air Pollution, and Human Health. *Curr. Environ. Health Rep.* **2018**, *5*, 179–186. [[CrossRef](#)] [[PubMed](#)]
2. Berry, H.L.; Waite, T.D.; Dear, K.B.G.; Capon, A.G.; Murray, V. The Case for Systems Thinking about Climate Change and Mental Health. *Nat. Clim. Chang.* **2018**, *8*, 282–290. [[CrossRef](#)]
3. Kattel, S.; Liu, P.; Chen, J.G. Tuning Selectivity of CO₂ Hydrogenation Reactions at the Metal/Oxide Interface. *J. Am. Chem. Soc.* **2017**, *139*, 9739–9754. [[CrossRef](#)] [[PubMed](#)]
4. Knutson, T.R.; Tuleya, R.E. Impact of CO₂-Induced Warming on Simulated Hurricane Intensity and Precipitation: Sensitivity to the Choice of Climate Model and Convective Parameterization. *J. Clim.* **2004**, *17*, 3477–3495. [[CrossRef](#)]
5. Schwiderowski, P.; Ruland, H.; Muhler, M. Current Developments in CO₂ Hydrogenation towards Methanol: A Review Related to Industrial Application. *Curr. Opin. Green Sustain. Chem.* **2022**, *38*, 100688. [[CrossRef](#)]
6. Xu, D.; Wang, Y.; Ding, M.; Hong, X.; Liu, G.; Tsang, S.C.E. Advances in Higher Alcohol Synthesis from CO₂ Hydrogenation. *Chem* **2021**, *7*, 849–881. [[CrossRef](#)]
7. Chatzilias, C.; Martino, E.; Zagoraios, D.; Kyriakou, G.; Katsaounis, A. Electrochemical Promotion of Catalysis for CO₂ Valorization. In *Recent Advances in Electrochemical Promotion of Catalysis; Modern Aspects of Electrochemistry*; Vernoux, P., Vayenas, C.G., Eds.; Springer: Cham, Switzerland, 2022; Volume 61.
8. Nozaki, F.; Sodesawa, T.; Satoh, S.; Kimura, K. Hydrogenation of Carbon Dioxide into Light Hydrocarbons at Atmospheric Pressure over Rh/Nb₂O₅ or Cu/SiO₂-Rh/Nb₂O₅. *J. Catal.* **1987**, *104*, 339–346. [[CrossRef](#)]
9. Solymosi, F.; Pasztor, M. Analysis of the R-Spectral Behavior of Adsorbed CO Formed in H₂ + CO₂ Surface Interaction over Supported Rhodium. *J. Catal.* **1987**, *104*, 312–322. [[CrossRef](#)]
10. Lapidus, A.L.; Gaidai, N.A.; Nekrasov, N.V.; Tishkova, L.A.; Agafonov, Y.A.; Myshenkova, T.N. The Mechanism of Carbon Dioxide Hydrogenation on Copper and Nickel Catalysts. *Pet. Chem.* **2007**, *47*, 91–98. [[CrossRef](#)]
11. Borodko, Y.; Somorjai, G.A. Catalytic Hydrogenation of Carbon Oxides—a 10-Year Perspective. *Appl. Catal. A Gen.* **1999**, *186*, 355–362. [[CrossRef](#)]
12. Kusama, H.; Kitamura Bando, K.; Okabe, K.; Arakawa, H. Effect of Metal Loading on CO₂ Hydrogenation Reactivity over Rh/SiO₂ Catalysts. *Appl. Catal.* **2000**, *197*, 255–268. [[CrossRef](#)]
13. Gasser, D.; Baiker, A. Hydrogenation of Carbon Dioxide over Copper-Zirconia Catalysts Prepared by In-Situ Activation of Amorphous Copper-Zirconium Alloy. *Appl. Catal.* **1989**, *48*, 279–294. [[CrossRef](#)]
14. Amenomiya, Y. Methanol synthesis from CO + H₂. II Copper-based binary and ternary catalysts. *Appl. Catal.* **1987**, *30*, 57–68. [[CrossRef](#)]
15. Sahibzada, M.; Chadwick, D.; Metcalfe, I.S. Hydrogenation of Carbon Dioxide to Methanol over Palladium-Promoted Cu/ZnO/A₁O₃ Catalysts. *Catal. Today* **1996**, *29*, 367–372. [[CrossRef](#)]
16. Solymosi, F.; Erdhelyi, A.; Bansagi, T. Methanation of CO, on Supported Rhodium Catalyst. *J. Catal.* **1981**, *68*, 371–382. [[CrossRef](#)]
17. Yang, R.; Zhang, Y.; Tsubaki, N. Dual Catalysis Mechanism of Alcohol Solvent and Cu Catalyst for a New Methanol Synthesis Method. *Catal. Commun.* **2005**, *6*, 275–279. [[CrossRef](#)]
18. Schild, C.; Wokaun, A.; Baiker, A. On the Mechanism of CO and CO₂ Hydrogenation Reactions on Zirconia-Supported Catalysts: A Diffuse Reflectance FTIR Study Part II. Surface Species on Copper/Zirconia Catalysts: Implications for Methanol Synthesis Selectivity. *J. Mol. Catal.* **1990**, *63*, 243–254. [[CrossRef](#)]
19. Vannice, M.A. The Catalytic Synthesis of Hydrocarbons from H₂CO Mixtures over the Group VIII Metals I. The Specific Activities and Product Distributions of Supported Metals. *J. Catal.* **1975**, *31*, 449–461. [[CrossRef](#)]
20. Araki, R.; Ponec, V. Methanation of Carbon Monoxide on Nickel and Nickel-Copper Alloys. *J. Catal.* **1976**, *44*, 439–448. [[CrossRef](#)]
21. Panagiotopoulou, P.; Kondarides, D.I.; Verykios, X.E. Selective Methanation of CO over Supported Noble Metal Catalysts: Effects of the Nature of the Metallic Phase on Catalytic Performance. *Appl. Catal. A Gen.* **2008**, *344*, 45–54. [[CrossRef](#)]
22. Henderson, A.; Worley, S.D.; Peebles, D.E. An Infrared Study of the Hydrogenation of Carbon Dioxide on Supported Rhodium Catalysts An inverse spillover effect. *J. Phys. Chem.* **1985**, *89*, 392–394. [[CrossRef](#)]

23. Solymosi, F.; Tombacz, I.; Koszta, J. Effects of Variation of Electric Properties of TiOp Support on Hydrogenation of CO and CO₂ over Rh Catalysts. *J. Catal.* **1985**, *95*, 578–586. [[CrossRef](#)]
24. Brown Bourzutschky, J.A.; Homs, N.; Bell, A.A.T. Hydrogenation of 002 and 002/00 Mixtures over Copper-Containing Catalysts. *J. Catal.* **1990**, *124*, 73–85. [[CrossRef](#)]
25. Chanchlani, K.G.; Hudgins, R.R.; Silveston, P.L. Methanol Synthesis from H₂, CO, and 002 over Cu/ZnO Catalysts. *J. Catal.* **1992**, *136*, 59–75. [[CrossRef](#)]
26. Nitta, Y.; Suwata, O.; Ikeda, Y.; Okamoto, Y.; Imanaka, T. Copper-Zirconia Catalysts for Methanol Synthesis from Carbon Dioxide: Effect of ZnO Addition to Cu-ZrO₂ Catalysts. *Catal. Lett.* **1994**, *26*, 345–354. [[CrossRef](#)]
27. Arena, F.; Italiano, G.; Barbera, K.; Bordiga, S.; Bonura, G.; Spadaro, L.; Frusteri, F. Solid-State Interactions, Adsorption Sites and Functionality of Cu-ZnO/ZrO₂ Catalysts in the CO₂ Hydrogenation to CH₃OH. *Appl. Catal. A Gen.* **2008**, *350*, 16–23. [[CrossRef](#)]
28. Reubroycharoen, P.; Vitidsant, T.; Yoneyama, Y.; Tsubaki, N. Development of a New Low-Temperature Methanol Synthesis Process. *Catal. Today* **2004**, *89*, 447–454. [[CrossRef](#)]
29. Hori, Y.; Wakebe, H.; Tsukamoto, T.; Koga, O. Adsorption of CO Accompanied with Simultaneous Charge Transfer on Copper Single Crystal Electrodes Related with Electrochemical Reduction of CO₂ to Hydrocarbons. *Surf. Sci.* **1995**, *335*, 258–260. [[CrossRef](#)]
30. Ando, H.; Xu, Q.; Fujiwara, M.; Matsumura, Y.; Tanaka, M.; Souma, Y. Hydrocarbon Synthesis from CO₂ over Fe ± Cu. *Catal. Today* **1998**, *45*, 229–234. [[CrossRef](#)]
31. Trovarelli, A.; Mustazza, C.; Dolcetti, G.; Kagpar, J.; Graziani, M. Carbon dioxide hydrogenation on rhodium supported on transition metal oxides. Effect of reduction temperature on product distribution. *Appl. Catal.* **1990**, *65*, 129–142. [[CrossRef](#)]
32. Marwood, M.; Doepper, R.; Renken, A. In-Situ Surface and Gas Phase Analysis for Kinetic Studies under Transient Conditions: The Catalytic Hydrogenation of CO₂. *Appl. Catal.* **1997**, *151*, 223–246. [[CrossRef](#)]
33. Falconer, J.L.; Zagli, A.E. Adsorption and Methanation of Carbon Dioxide on a Nickel/Silica Catalyst. *J. Catal.* **1980**, *62*, 280–285. [[CrossRef](#)]
34. Biloen, P.; Helle, J.N.; Van Den Berg, F.G.A.; Sachtleber, W.M.H. On the Activity of Fischer-Tropsch and Methanation Catalysts: A Study Utilizing Isotopic Transients. *J. Catal.* **1983**, *81*, 450–463. [[CrossRef](#)]
35. Coenen, J.W.E.; Van Nisselrooy, P.F.M.T.; De Croon, M.H.J.M.; Van Dooren, P.F.H.A.; Van Meerten, R.Z.C. The dynamics of methanation of carbon monoxide on Nickel catalysts. *Appl. Catal.* **1986**, *25*, 1–8. [[CrossRef](#)]
36. Zheng, Y.; Zhang, J.; Ma, Z.; Zhang, G.; Zhang, H.; Fu, X.; Ma, Y.; Liu, F.; Liu, M.; Huang, H. Seeded Growth of Gold–Copper Janus Nanostructures as a Tandem Catalyst for Efficient Electroreduction of CO₂ to C₂₊ Products. *Small* **2022**, *18*, 2201695. [[CrossRef](#)]
37. Zhong, Y.; Kong, X.; Song, Z.; Liu, Y.; Peng, L.; Zhang, L.; Luo, X.; Zeng, J.; Geng, Z. Adjusting Local CO Confinement in Porous-Shell Ag@Cu Catalysts for Enhancing C-C Coupling toward CO₂ Electroreduction. *Nano Lett.* **2022**, *22*, 2554–2560. [[CrossRef](#)]
38. Vayenas, C.G.; Bebelis, S.; Pliangos, C.; Brosda, S.; Tsiplakides, D. *Electrochemical Activation of Catalysis Promotion, Electrochemical Promotion, and Metal-Support Interactions*; Springer: New York, NY, USA, 2002.
39. Theleritis, D.; Souentie, S.; Siokou, A.; Katsaounis, A.; Vayenas, C.G. Hydrogenation of CO₂ over Ru/YSZ Electropromoted Catalysts. *ACS Catal.* **2012**, *2*, 770–780. [[CrossRef](#)]
40. Kalaitzidou, I.; Makri, M.; Theleritis, D.; Katsaounis, A.; Vayenas, C.G. Comparative Study of the Electrochemical Promotion of CO₂ Hydrogenation on Ru Using Na⁺, K⁺, H⁺ and O²⁻ Conducting Solid Electrolytes. *Surf. Sci.* **2016**, *646*, 194–203. [[CrossRef](#)]
41. Panaritis, C.; Michel, C.; Couillard, M.; Baranova, E.A.; Steinmann, S.N. Elucidating the Role of Electrochemical Polarization on the Selectivity of the CO₂ Hydrogenation Reaction over Ru. *Electrochim. Acta* **2020**, *350*, 136405. [[CrossRef](#)]
42. Chatzilias, C.; Martino, E.; Tsatsos, S.; Kyriakou, G.; Katsaounis, A.; Vayenas, C.G. Kinetic study of CO₂ hydrogenation on Ru/YSZ catalyst using a monolithic electropromoted reactor (MEPR). *Chem. Eng. J.* **2022**, *430*, 132967. [[CrossRef](#)]
43. Zagoraios, D.; Panaritis, C.; Krassakopoulou, A.; Baranova, E.A.; Katsaounis, A.; Vayenas, C.G. Electrochemical Promotion of Ru Nanoparticles Deposited on a Proton Conductor Electrolyte during CO₂ Hydrogenation. *Appl. Catal. B* **2020**, *276*, 119148. [[CrossRef](#)]
44. Bebelis, S.; Karasali, H.; Vayenas, C.G. Electrochemical Promotion of CO₂ Hydrogenation on Rh/YSZ Electrodes. *J. Appl. Electrochem.* **2008**, *38*, 1127–1133. [[CrossRef](#)]
45. Papaioannou, E.I.; Souentie, S.; Hammad, A.; Vayenas, C.G. Electrochemical Promotion of the CO₂ Hydrogenation Reaction Using Thin Rh, Pt and Cu Films in a Monolithic Reactor at Atmospheric Pressure. *Catal. Today* **2009**, *146*, 336–344. [[CrossRef](#)]
46. Kotsiras, A.; Kalaitzidou, I.; Grigoriou, D.; Symillidis, A.; Makri, M.; Katsaounis, A.; Vayenas, C.G. Electrochemical Promotion of Nanodispersed Ru-Co Catalysts for the Hydrogenation of CO₂. *Appl. Catal. B* **2018**, *232*, 60–68. [[CrossRef](#)]
47. Panaritis, C.; Zgheib, J.; Ebrahim, S.A.H.; Couillard, M.; Baranova, E.A. Electrochemical In-Situ Activation of Fe-Oxide Nanowires for the Reverse Water Gas Shift Reaction. *Appl. Catal. B* **2020**, *269*, 118826. [[CrossRef](#)]
48. Nicole, J.; Comminellis, C.; Tsiplakides, D.; Pliangos, C.; Verykios, X.E.; Vayenas, C.G. Electrochemical Promotion and Metal-Support Interactions. *J. Catal.* **2001**, *204*, 23–34. [[CrossRef](#)]
49. Stoukides, M.; Vayenas, C.G. The Effect of Electrochemical Oxygen Pumping on the Rate and Selectivity of Ethylene Oxidation on Polycrystalline Silver. *J. Catal.* **1981**, *70*, 137–146. [[CrossRef](#)]
50. Vayenas, C.G.; Koutsodontis, C.G. Non-Faradaic Electrochemical Activation of Catalysis. *J. Chem. Phys.* **2008**, *128*, 182506. [[CrossRef](#)]

51. Vayenas, C.G.; Bebelis, S.; Ladas, S. Dependence of Catalytic Rates on Catalyst Work Function. *Nature* **1990**, *343*, 625–627. [[CrossRef](#)]
52. Bebelis, S.; Vayenas, C.G. Non-Faradaic Electrochemical Modification of Catalytic Activity 1. The Case of Ethylene Oxidation on Pt. *J. Catal.* **1989**, *118*, 125–146. [[CrossRef](#)]
53. Vayenas, C.G.; Bebelis, S.; Despotopoulou, M. Non-Faradaic Electrochemical Modification of Catalytic Activity 4. The Use of B"-Al₂O₃ as the Solid Electrolyte. *J. Catal.* **1991**, *128*, 415–435. [[CrossRef](#)]
54. Ladas, S.; Bebelis, S.; Vayenas, C.G. Work Function Measurements on Catalyst Films Subject to in Situ Electrochemical Promotion. *Surf. Sci.* **1991**, *251–252*, 1062–1068. [[CrossRef](#)]
55. Neophytides, S.G.; Tsipakides, D.; Stonehart, P.; Jaksic, M.M.; Vayenas, C.G. Electrochemical Enhancement of a Catalytic Reaction in Aqueous Solution. *Nature* **1994**, *370*, 45–47. [[CrossRef](#)]
56. Pliangos, C.; Raptis, C.; Badas, T.; Tsipakides, D.; Vayenas, C.G. Electrochemical Promotion of a Classically Promoted Rh Catalyst for the Reduction of NO. *Electrochim. Acta* **2000**, *46*, 331–339. [[CrossRef](#)]
57. Vernoux, P.; Gaillard, F.; Bultel, L.; Siebert, E.; Primet, M. Electrochemical Promotion of Propane and Propene Oxidation on Pt/YSZ. *J. Catal.* **2002**, *208*, 412–421. [[CrossRef](#)]
58. Katsaounis, A.; Teschner, D.; Zafeiratos, S. The Effect of Polarization and Reaction Mixture on the Rh/YSZ Oxidation State During Ethylene Oxidation Studied by Near Ambient Pressure XPS. *Top. Catal.* **2018**, *61*, 2142–2151. [[CrossRef](#)]
59. Constantinou, I.; Archonta, D.; Brosda, S.; Lepage, M.; Sakamoto, Y.; Vayenas, C.G. Electrochemical Promotion of NO Reduction by C₃H₆ on Rh Catalyst-Electrode Films Supported on YSZ and on Dispersed Rh/YSZ Catalysts. *J. Catal.* **2007**, *251*, 400–409. [[CrossRef](#)]
60. Souentie, S.; Xia, C.; Falgairette, C.; Li, Y.D.; Comninellis, C. Investigation of the “Permanent” Electrochemical Promotion of Catalysis (P-EPOC) by Electrochemical Mass Spectrometry (EMS) Measurements. *Electrochim. Commun.* **2010**, *12*, 323–326. [[CrossRef](#)]
61. Falgairette, C.; Jaccoud, A.; Fóti, G.; Comninellis, C. The Phenomenon of “Permanent” Electrochemical Promotion of Catalysis (P-EPOC). *J. Appl. Electrochem.* **2008**, *38*, 1075–1082. [[CrossRef](#)]
62. Kokka, A.; Petala, A.; Panagiotopoulou, P. Support Effects on the Activity of Ni Catalysts for the Propane Steam Reforming Reaction. *Nanomaterials* **2021**, *11*, 1948. [[CrossRef](#)]
63. Yentekakis, I.V.; Goula, G.; Panagiotopoulou, P.; Kampouri, S.; Taylor, M.J.; Kyriakou, G.; Lambert, R.M. Stabilization of Catalyst Particles against Sintering on Oxide Supports with High Oxygen Ion Lability Exemplified by Ir-Catalyzed Decomposition of N₂O. *Appl. Catal. B* **2016**, *192*, 357–364. [[CrossRef](#)]
64. Blomberg, S.; Lundgren, E.; Westerström, R.; Erdogan, E.; Martin, N.M.; Mikkelsen, A.; Andersen, J.N.; Mittendorfer, F.; Gustafson, J. Structure of the Rh₂O₃(0001) Surface. *Surf. Sci.* **2012**, *606*, 1416–1421. [[CrossRef](#)]
65. Holzwarth, U.; Gibson, N. The Scherrer Equation versus the “Debye-Scherrer Equation”. *Nat. Nanotechnol.* **2011**, *6*, 534. [[CrossRef](#)] [[PubMed](#)]
66. Jiménez-Borja, C.; De Lucas-Consuegra, A.; Sapountzi, F.; Dorado, F.; Katsaounis, A.; Valverde, J.L. Oscillatory Behavior of Rh/YSZ under Electropromoted Conditions. *Chem. Phys. Lett.* **2012**, *519–520*, 89–92. [[CrossRef](#)]
67. Hamdy, M.S.; Alhanash, A.M.; Benissa, M.; Alsalme, A.; Alharthi, F.A.; Al-Zaqri, N. Rhodium Nanoparticles Incorporated Mesoporous Silica as an Active Catalyst for Cyclohexene Hydrogenation under Ambient Conditions. *Catalysts* **2020**, *10*, 925. [[CrossRef](#)]
68. Tsatsos, S.; Kyriakou, G. Copper Growth on a Stepped Nickel Surface: Electronic and Geometric Effects on CO Reactivity. *J. Phys. Chem.* **2023**, *127*, 6337–6346. [[CrossRef](#)]

Disclaimer/Publisher’s Note: The statements, opinions and data contained in all publications are solely those of the individual author(s) and contributor(s) and not of MDPI and/or the editor(s). MDPI and/or the editor(s) disclaim responsibility for any injury to people or property resulting from any ideas, methods, instructions or products referred to in the content.